Journal of Applied Physics

Investigation of wurtzite formation in MOVPE-grown zincblende GaN epilayers on $Al_xGa_{1-x}N$ nucleation layers

Cite as: J. Appl. Phys. **131**, 115703 (2022); https://doi.org/10.1063/5.0077186
Submitted: 31 October 2021 • Accepted: 21 February 2022 • Published Online: 17 March 2022

Abhiram Gundimeda, Martin Frentrup, Simon M. Fairclough, et al.

Journal of Applied Physics ARTICLE scitation.org/journal/jap

Investigation of wurtzite formation in MOVPE-grown zincblende GaN epilayers on $Al_xGa_{1-x}N$ nucleation layers

Cite as: J. Appl. Phys. **131**, 115703 (2022); doi: 10.1063/5.0077186
Submitted: 31 October 2021 · Accepted: 21 February 2022 ·
Published Online: 17 March 2022

Abhiram Gundimeda,[1,a)] Martin Frentrup,[1] Simon M. Fairclough,[1] Menno J. Kappers,[1] David J. Wallis,[1,2] and Rachel A. Oliver[1]

AFFILIATIONS

[1]Department of Materials Science and Metallurgy, University of Cambridge, 27 Charles Babbage Rd., Cambridge CB3 0FS, United Kingdom
[2]Centre for High Frequency Engineering, University of Cardiff, 5 The Parade, Newport Road, Cardiff CF24 3AA, United Kingdom

Note: This paper is part of the Special Topic on Defects in Semiconductors.
[a)]**Author to whom correspondence should be addressed:** ag2025@cam.ac.uk

ABSTRACT

The influence of AlGaN nucleation layers on zincblende GaN epilayers was studied to investigate the formation of wurtzite phase inclusions in the epilayer. GaN epilayers grown on AlGaN nucleation layers with varying aluminum contents suffer from the increasing presence of wurtzite inclusions as the aluminum content of the nucleation layer increases. High-resolution transmission electron microscopy along with four-dimensional scanning transmission electron microscopy is used to investigate the origin of the wurtzite inclusions in the nucleation layer and at the GaN/AlGaN interface. It was observed that a GaN nucleation layer and an $Al_{0.95}Ga_{0.05}N$ nucleation layer grew in the zincblende and wurtzite phase, respectively. These phases were then adopted by the overgrown GaN epilayers. For a GaN epilayer on an $Al_{0.29}Ga_{0.71}N$ nucleation layer, wurtzite inclusions tend to form at the GaN/ $Al_{0.29}Ga_{0.71}N$ interface due to strong {111}-type faceting observed in the zincblende nucleation layer. This strong faceting is correlated with an enrichment of aluminum in the upper part of the nucleation layer, as observed in energy dispersive x-ray spectroscopy, which may influence the kinetics or thermodynamics controlling the surface morphology.

I. INTRODUCTION

GaN-based (opto)electronics have achieved commercial success over the last two decades due to their superior physical and optical properties, such as high electron mobility, high electron saturation velocity, and variable bandgap.[1,2] However, while conventional wurtzite InGaN-based LEDs emitting in the blue spectral region have high internal quantum efficiencies,[3] the efficiency of green wavelength nitride LEDs is nearly a factor of two lower.[4] This so-called "green gap" problem is caused by the presence of spontaneous and piezoelectric polarization fields in hexagonal wurtzite (wz) group III-nitrides in the [0001] growth direction. These fields result in a reduced overlap of the electron–hole wave functions in the active region and a low radiative recombination efficiency, known as the quantum confined Stark effect. Using the cubic zincblende (zb) phase can potentially overcome these hurdles due to the absence of both spontaneous and piezoelectric polarization in the (001) orientation.[5,6] Also, the bandgap of zb-InGaN is smaller than that of wz-InGaN of similar composition so that less In incorporation is required to achieve green emission. However, the zb III-nitrides are thermodynamically metastable so that phase pure growth with low defect density is a challenge.

Zb-GaN is usually heteroepitaxially grown on foreign substrates, such as Si, Al_2O_3, SiC, etc., leading to lattice mismatch and thermal expansion coefficient (TEC) mismatch between the materials, which can give rise to the formation of defects.[7] To compensate for these mismatches, extensive studies have been carried out on

the growth of zb-GaN via both metal organic vapor phase epitaxy (MOVPE) and molecular beam epitaxy (MBE) on various substrates, such as GaAs[8–12] and 3C-SiC/Si.[13–16] 3C-SiC is the most promising substrate due to its thermal stability under growth conditions and its moderate lattice mismatch (3.4% with GaN; 0.3% with AlN). However, this lattice mismatch, together with the TEC mismatch of the materials involved, can be a challenge for the development of large scale zb-GaN templates for green emitting devices. Similar mismatch issues were overcome in conventional wz-GaN growth on Si (111) by utilizing AlN nucleation layers (NLs) and graded $Al_xGa_{1-x}N$ buffer layers, with intermediate lattice constants between GaN and the substrate to achieve strain management.[17]

In this context, the use of zb-$Al_xGa_{1-x}N$ NLs, which in theory allow for lattice mismatches with 3C-SiC of only 0.3% in the case of AlN, was investigated in a previous study.[18] It was found that the GaN epilayer was highly zb phase pure when grown on $Al_xGa_{1-x}N$ NLs with low Al contents (<2%) but deteriorating quickly for higher Al contents. The origin of this phase change in intended cubic GaN films grown on $Al_xGa_{1-x}N$ NLs is not understood. While transmission electron microscopy (TEM) studies have revealed a very high phase purity and no pronounced faceting of individual zb-GaN islands,[7] the change in the growth conditions required to allow alloying of the NLs with Al could promote the formation of {111} facets, which may act as nucleation sites for wz inclusions and stacking faults (SFs).[19,20] Hence, a selection of samples grown using the method described in Ref. 18 were chosen for a detailed electron microscopy (EM) study including transmission electron microscopy (TEM), scanning transmission electron microscopy (STEM), and four-dimensional STEM (4D-STEM). To understand the origin of the wz inclusions in the GaN epilayers, we focused on any local faceting at the $Al_xGa_{1-x}N$/3C-SiC and the GaN/ $Al_xGa_{1-x}N$ interfaces, as well as the alloy distribution across the $Al_xGa_{1-x}N$ NLs.

II. EXPERIMENTAL DETAILS

The $Al_xGa_{1-x}N$ NLs and GaN epilayers investigated here were the same as those reported in Ref. 18. In brief, first, a 15 nm thick $Al_xGa_{1-x}N$ NLs with varying alloy composition was grown at about 600 °C by MOVPE in a 6×2 in. Thomas Swan close-coupled showerhead reactor on cubic 3C-SiC/Si (001) pseudo-substrates with a nominal 4° miscut toward the [110] in-plane direction. The $Al_xGa_{1-x}N$ NLs then underwent a thermal treatment in an atmosphere of NH_3 and H_2 while ramping the temperature to the epilayer growth conditions. Following the AlGaN NLs, a further 600 nm thick GaN epilayer was grown at a temperature of about 880 °C. In this study, three samples with $x = 0.0$, 0.29 ± 0.02, and 0.95 ± 0.02 in the $Al_xGa_{1-x}N$ NLs were chosen to be investigated as these had shown strong differences in the morphologic and structural properties of the GaN epilayer.[18] The composition of these samples has been measured by x-ray photoelectron spectroscopy, which is known to be a surface sensitive technique allowing reasonably accurate measurement of the composition of the thin NLs. The phase purity of these samples has been determined by x-ray diffraction (XRD) using the integrated intensities of the 113 zb-GaN reflection and the 1-103 wz-GaN reflection following the description in Ref. 21.

For the structural EM analysis, cross-sectional thin foils were prepared using a FEI Helios NanoLab™ focused ion beam (FIB) microscope for *in situ* lift-out using 1 μm Pt metal to protect the surface, followed by Ga ion milling at 30 kV and a final 5 kV treatment to reduce ion damage to make a lamella of about 80–120 nm thickness. The annealed AlGaN NL, for TEM imaging, was prepared by initial electron deposition of a few nanometers of carbon for better image contrast. High-resolution transmission electron microscopy (HRTEM) images were obtained from a FEI Techani F20 microscope operated at 200 kV. 4D-STEM measurements were performed at 200 kV in the STEM mode on this instrument with a NanoMegas DigiSTAR diffraction system and processed using software package Pyxem.[22] 4D-STEM phase maps were generated by matching the measured diffraction patterns at each pixel (3×3 nm^2) against simulated diffraction patterns for both the zinc-blende and the wurtzite phases. Furthermore, high-angle annular dark-field (HAADF) STEM imaging and energy dispersive x-ray spectroscopy (EDS) measurements of as-grown and annealed $Al_xGa_{1-x}N$ NLs only were taken on a FEI Tecnai Osiris microscope, operated at 200 kV with a beam current of 80 pA and equipped with a high-brightness XFEG source and four-EDS-detector SuperX system. All the TEM/STEM measurements for each sample were taken across a few micrometers of film with the beam direction parallel to the [110] zone axis. Atomic force microscopy (AFM) measurements were performed using Bruker Dimension Icon Pro in PeakForce tapping mode using Bruker SCANASYST-AIR tips. The fast scan direction was aligned along the [110] miscut direction for all samples.

III. RESULTS AND DISCUSSION

A. Microstructural characterization of GaN on GaN NLs (x = 0.0)

The microstructural properties of the GaN epilayer grown with a GaN NL, for which XRD analyses have previously shown to have a zb phase purity above 90%,[18] are discussed first. To gain an insight into the phase distribution at the interfaces, HRTEM was used to investigate the two interfaces between the epilayer, NL, and SiC substrate. Figure 1(a) shows the cross-sectional HRTEM image of both interfacial regions. A closer look at the GaN/SiC interface indicates that the surface of the 3C-SiC is smooth with small surface steps occasionally.

A 2D-fast Fourier transform (FFT) analysis was performed across different regions in each layer, revealing consistent data within each layer. The FFT patterns taken from red square regions are representative of each layer. The 2D-FFT pattern obtained in the 3C-SiC region shows intense and sharp spots [Fig. 1(b)], indicating that the material has a highly crystalline zb structure with (001) surface orientation. These structural properties were maintained in the GaN NL and the GaN epilayer as evidenced by the FFT patterns in Figs. 1(c) and 1(d). Indeed, we have not observed any wurtzite phase in the NL and epilayer across several micrometers of film, which highlights the high phase purity of the zb-GaN NL and the GaN epilayer. In the FFT patterns of the GaN NL and the GaN epilayer, bright streaks along the ⟨111⟩ directions can be

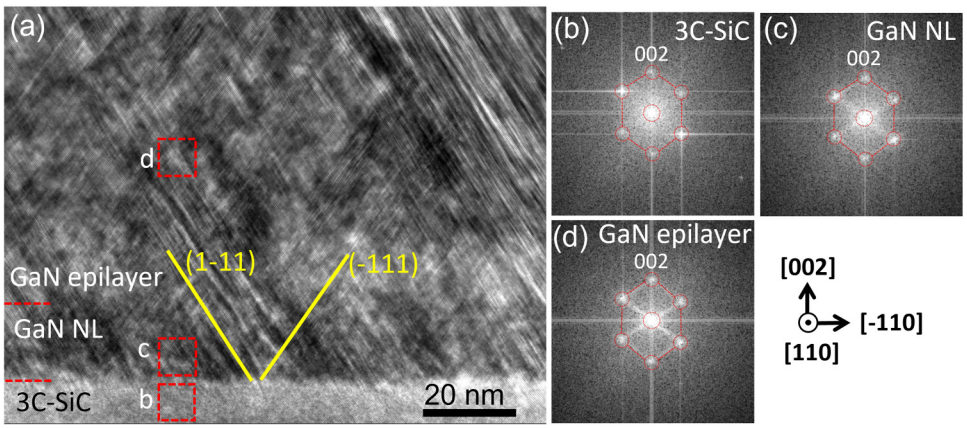

FIG. 1. (a) Cross-sectional HRTEM image (zone axis = [110]) of the zb-GaN epilayer on GaN NL grown over 3C-SiC. The 2D-FFT images are taken from the red colored boxes in (a) labeled as (b) 3C-SiC, (c) GaN NL, and (d) GaN epilayer.

seen across the FFT spots, which are attributed to a high density of stacking faults on the close-packed {111} planes. In the HRTEM image in Fig. 1(a), examples of (–111) and (1–11) SFs are highlighted with solid yellow lines, which are both inclined at 55° from the GaN/SiC interface (red dotted line). From the HRTEM image, it is observed that the majority of these stacking faults originate from the GaN/3C-SiC interface. Most of the SFs annihilate within the first few tens of nanometers so that the total SF density reduces drastically, as have been studied in detail for a GaN/GaN sample, similar to the sample in this study by Vacek *et al.*[7] and Lee *et al.*[23] However, in some cases, bunches of parallel SFs [like in the top right corner of Fig. 1(a)] extend into the GaN epilayer.

Detailed electron microscopic analysis by Vacek *et al.* revealed that the lattice mismatch between the GaN NL and the 3C-SiC leads to the formation of misfit dislocations at the interface, which dissociates into partial dislocations connected by stacking faults.[7] In Fig. 1(a), the density of SFs reduces with increasing film thickness by reaction and annihilation of SFs of different {111} planes. The observations highlight that the GaN epilayer grown on GaN NL is fully zb in phase with a high density of stacking faults in the GaN NL and GaN epilayer.

B. GaN on $Al_xGa_{1-x}N$ NLs with high Al composition (x = 0.95)

For the sample with an $Al_{0.95}Ga_{0.05}N$ NL, the XRD phase analysis revealed that the GaN epilayer is fully wz in phase.[18] To investigate the origin of the wz phase, high-resolution TEM images, such as those shown in Fig. 2(a), were taken. The 2D-FFT pattern obtained from 3C-SiC [Fig. 2(b)] indicates that the substrate is highly crystalline with no stacking faults in this region. However, the 2D-FFT pattern obtained from the $Al_{0.95}Ga_{0.05}N$ NL [Fig. 2(c)] shows a characteristic pattern of the wz phase. This reveals that the wz phase formation initiates from the onset of the NL growth. A possible explanation for the strong tendency of AlN toward the wz phase might be related to the theoretically predicted larger difference of the total energy between the zb and wz phase in AlN compared to GaN.[24] When comparing the 2D-FFT patterns of $Al_{0.95}Ga_{0.05}N$ NL and 3C-SiC [Figs. 2(b) and 2(c)], the 0002 $Al_{0.95}Ga_{0.05}N$ reflection matches the position of one of the 111 3C-SiC reflections. This shows that the crystallographic relation between the close-packed planes of the zb and wz phases is $(111)_{zb} \parallel (0001)_{wz}$ and $[110]_{zb} \parallel [11\text{-}20]_{wz}$, as they only differ in the stacking sequence. Following the NL further up the heterostructure,

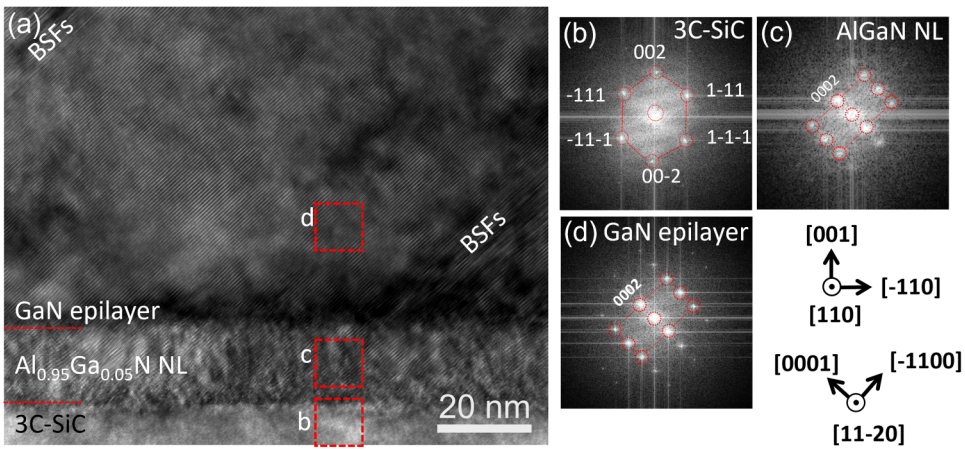

FIG. 2. (a) Cross-sectional HRTEM image (zone axis = [110]) of the zb-GaN epilayer on $Al_{0.95}Ga_{0.05}N$ NL grown on 3C-SiC. The 2D- FFT images are taken from the red colored boxes in (a) labeled as (b) 3C-SiC (c) $Al_{0.95}Ga_{0.05}N$ NL, and (d) GaN epilayer.

the interface between $Al_{0.95}Ga_{0.05}N$ NL and GaN epilayer appears relatively smooth. The overgrown GaN epilayer has the same semi-polar (3-304) growth orientation as the NL with the wz phase, which is evident from the 2D-FFT pattern obtained [Fig. 2(d)] in the epilayer and the characteristic lattice interference fringes in the HRTEM image. Interestingly, relatively large sections (>100 nm) of the GaN film appear nearly perfect with no or nearly no basal plane stacking faults (BSFs). Such bunches of (0001) BSFs are, for example, shown in the top left and bottom right parts in Fig. 2(a).

C. GaN on $Al_xGa_{1-x}N$ NLs with intermediate Al composition (x = 0.29)

The results in Secs. III B and III C have shown that the GaN epilayer grown on a GaN NL is fully zb in phase (Fig. 1), while the GaN epilayer grown on an $Al_{0.95}Ga_{0.05}N$ NL is fully wz in phase (Fig. 2). XRD results indicate that the GaN epilayer starts to exhibit mixed phases, with 44% zb phase, when grown on $Al_xGa_{1-x}N$ NLs with an intermediate composition of about $x \approx 0.29$.[18] To explore the distribution of the wz regions in this mixed phase sample, 4D-STEM measurements were performed. Figure 3(a) shows a virtual bright field image of the zb-GaN epilayer on $Al_{0.29}Ga_{0.71}N$ NL and its corresponding phase map in Fig. 3(b). In the phase map, the zb phase of GaN is indicated in green and the wz phase in red. Small areas shown in yellow are highly defective regions, which do not clearly relate to either phase. Typical diffraction patterns recorded from these regions are shown in Figs. 3(c)–3(e). The 4D-STEM phase map is consistent with our previously reported XRD data in showing that the GaN epilayer is a mixture of zb and wz phases, in which columnar-like wz regions are inclined. Here, the proportions of the zb and wz phases do not systematically

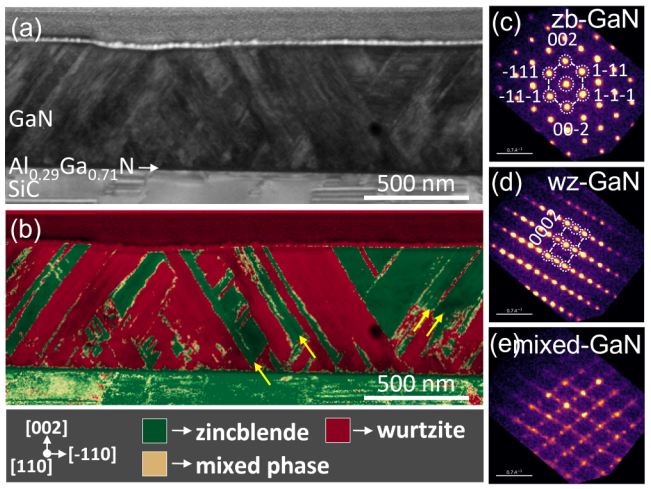

FIG. 3. (a) Virtual bright field image (zone axis = [110]) of the zb-GaN epilayer on $Al_{0.29}Ga_{0.71}N$ NL grown on 3C-SiC (b) corresponding 4D-STEM phase map overlapped on the virtual bright field image. The green color indicates the zb phase, the red color indicates the wz phase, and the pale-yellow color indicates the mixed phase. The 2D-FFTs are taken from the regions of (c) zb-GaN, (d) wz-GaN, and (e) mixed phases in the GaN epilayer.

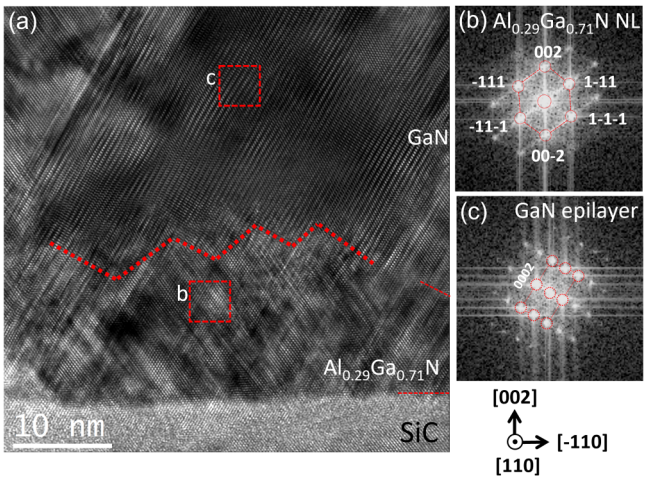

FIG. 4. (a) Cross-sectional HRTEM image (zone axis = [110]) of the zb-GaN epilayer on $Al_{0.29}Ga_{0.71}N$ NL grown on 3C-SiC. The 2D-FFTs are taken from the regions of (b) $Al_{0.29}Ga_{0.71}N$ NL and (c) GaN epilayer.

change from the interface to the surface. However, the volume of material analyzed here is much lower than in XRD so that any quantitative analysis of the phase purity from such a 4D-STEM image will suffer from poor statistical relevance. Looking at the details in Fig. 3(b), the regions with zb phase have a high density of (1−11) and (−111) stacking faults that are going across the epilayer from the interface, guided by yellow arrows. The orientation of the boundaries of the wz regions matches the orientation of the (−111) and (1−11) SFs, indicating that stacking errors might be acting as

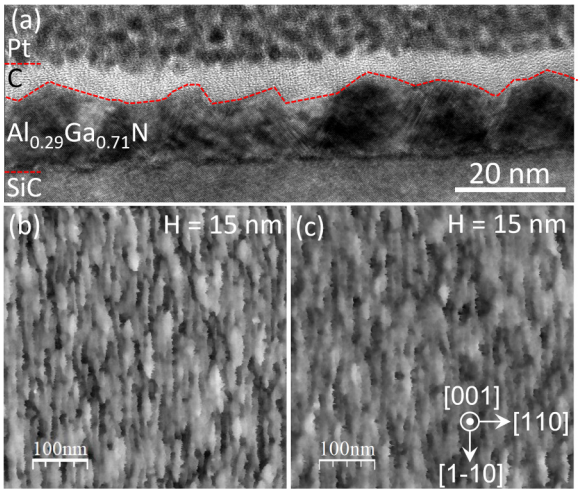

FIG. 5. (a) Cross-sectional HRTEM image (zone axis = [110]) of the annealed $Al_{0.29}Ga_{0.71}N$ NL grown on 3C-SiC. AFM images of (b) as-grown and (c) annealed $Al_{0.29}Ga_{0.71}N$ NLs.

the origin point for the wz regions to grow in the [0001] direction in the wz epilayer. While these 4D-STEM phase maps are helpful to identify the regions of the wz phases in the epilayer, no detailed conclusion on their origin can be obtained as the nucleation region is too thin to differentiate the phases within it at the limited 4D-STEM map resolution.

In order to identify the location where the wz inclusions originate, HRTEM measurements were performed at the interfacial regions between 3C-SiC substrate, $Al_{0.29}Ga_{0.71}N$ NL, and GaN epilayer, as shown in Fig. 4. The 2D-FFT pattern obtained from the $Al_{0.29}Ga_{0.71}N$ NL shows it to be of the zb phase [Fig. 4(b)], albeit with the influence of SFs seen as streaks crossing the diffraction spots. These observations are evident across several micrometers of sample width, of which only a small section is shown here, indicating that the majority of the NL is of the zb phase and no extended wz inclusions were formed in the NL region. Immediately above the defective $Al_{0.29}Ga_{0.71}N$ NL, a region of GaN with distinctive wz stacking can be observed, which is also evident from the

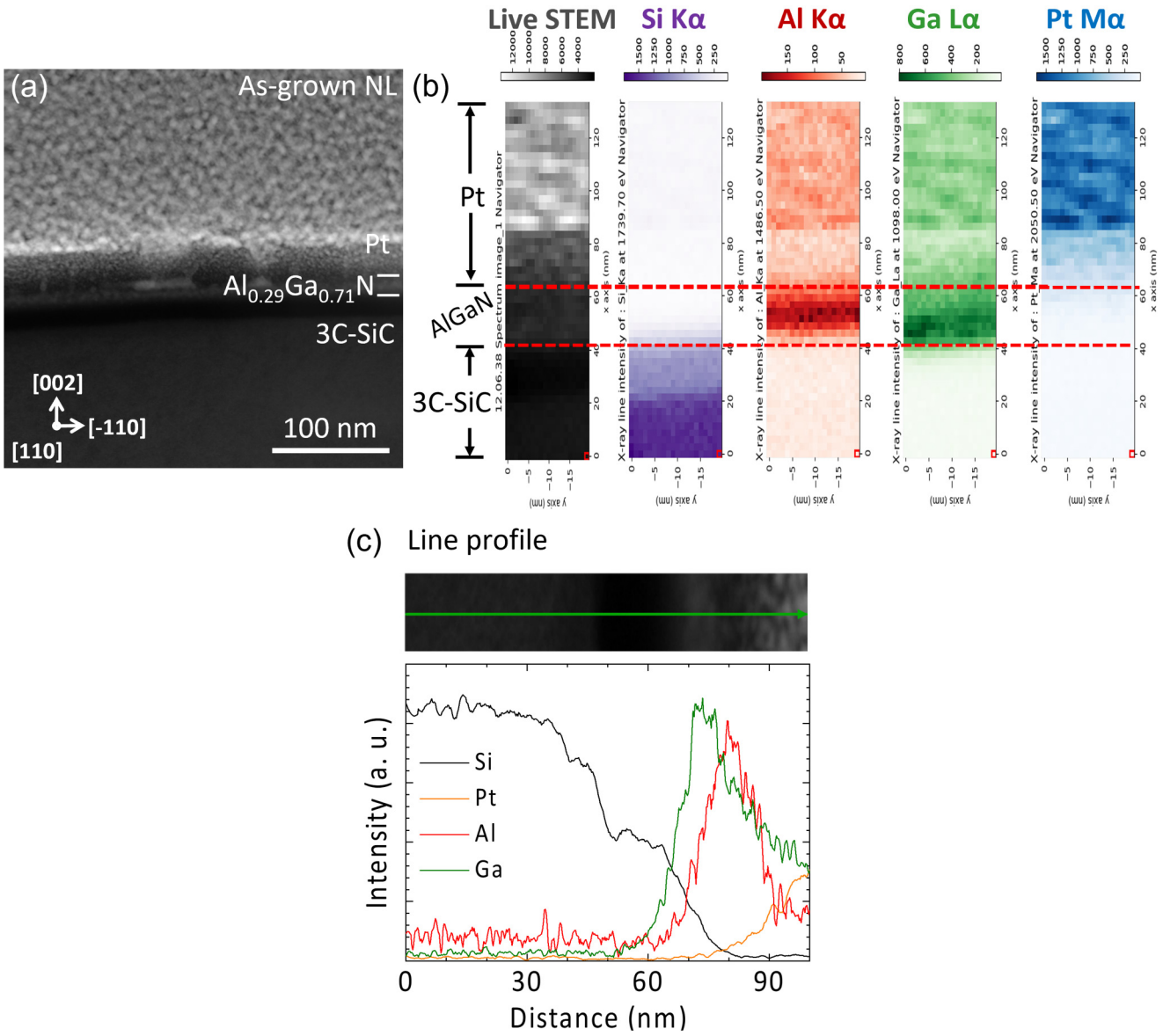

FIG. 6. (a) STEM image (zone axis = [110]) of as-grown $Al_{0.29}Ga_{0.71}N$ NL grown on 3C-SiC. (b) The corresponding STEX-EDX elemental intensity maps of Si Kα, Al Kα, Ga Lα, Pt Mα, and live STEM image. (c) Line profile taken across the NL.

characteristic wz GaN 2D-FFT pattern in Fig. 4(c). This suggests that the wz GaN material in the epilayer originates at the AlGaN/GaN interface. However, even though a relatively large area of the NL has been examined, the presence of some wurtzite material in the NL cannot be ruled out completely. Hence, it remains possible that small regions of wz are present in the NL and grow laterally to dominate the overlying epilayer, but that we do not observe them within our studies. However, this seems unlikely to be the dominant source, and a stronger candidate for the nucleation of the wz phase in the GaN epilayer is the strong faceting at the $Al_{0.29}Ga_{0.71}N$/GaN interface as highlighted by the broken red line in Fig. 4(a). An analysis of these facets revealed facet angles of about 55° with the (001) growth plane, which suggests that these facets are predominately {111} close-packed planes. Such exposed {111} facets may promote the growth of wz inclusions as has been noted by Lorenz *et al.* and Wei *et al.*[19,20] High-resolution imaging of the annealed AlGaN NL sample without overgrown GaN also reveals significant surface faceting with high density of stacking faults in the region [Fig. 5(a)]. Even though such a trend is observed across a few micrometers of the TEM specimen, the complete absence of the wz phase in the NLs cannot be ruled out fully. In Fig. 5, AFM images of the as-grown (b) and the annealed (c) $Al_{0.29}Ga_{0.71}N$ NLs reveal a very similar surface morphology with elongated grains with increased size in the annealed $Al_{0.29}Ga_{0.71}N$ NL as compared to as-grown $Al_{0.29}Ga_{0.71}N$ NL. This suggests that the strong faceting observed in cross-sectional TEM images may be formed during the growth of the NLs prior to the high temperature treatment. The growth studies of zb-GaN epilayers by Lee *et al.* have shown that the density and the size of low index facets like {111} strongly depend on the growth conditions.[16] For example, higher V/III ratios tend to lead to more (111) facet formation and a higher portion of wz inclusions. Hence, further optimization of the growth parameters for $Al_xGa_{1-x}N$ growth, at high Al contents, may allow us to obtain smoother NLs and improved phase purity in epilayers.

Last, STEM-EDX measurements were performed on an as-grown and an annealed $Al_{0.29}Ga_{0.71}N$ NL were investigated for any variation in the alloy distribution. Figure 6 shows the STEM-EDX measurements [Fig. 6(a)] of the as-grown $Al_{0.29}Ga_{0.71}N$ NL and the corresponding elemental maps [Fig. 6(b)] of Si (purple), Al (red), and Ga (green) obtained from this region. The elemental maps for Si and Pt were collected as markers for the 3C-SiC substrate and the Pt-covered surface. The STEM-EDX elemental maps of the NL reveal that the distribution of Al and Ga is non-uniform across the NL. The as-grown NL is Ga enriched near to the $Al_xGa_{1-x}N$/3C-SiC interface and contains an increased Al content toward the surface of the NL. This is confirmed by the line profile obtained across the NL in Fig. 6(c), where a clear variation in intensities of the Al and Ga signals can be observed with the Al-profile being shifted by about (6 ± 2) nm related to the Ga-profile. Close to the surface region, the Pt signal immediately rises as the Al signal reaches near zero. This implies that the surface region might be Ga coated or Ga beam damaged during the FIB sample preparation. Therefore, the data in the surface region are not interpretable. A similar non-uniform distribution of Al and Ga across the nucleation region as has been observed for the annealed NL sample (see supplementary material), showing that the observed uneven alloy concentration is solely related to the growth of the NL and not related to the high temperature thermal treatment or the overgrowth with GaN. A plausible explanation could be a delayed Al incorporation into the $Al_xGa_{1-x}N$ NL caused by differences in the decomposition times of the metal organic precursors at the SiC surface. A slower decomposition of trimethylaluminum (TMAl) compared to trimethylgallium (TMGa) might arise from the high tendency of TMAl to particle formation[25] and a larger number of decomposition steps for the formation of Al radicals in the case of TMAl.[26,27] Furthermore, the increasing formation of {111} facets for thicker NLs might lead to a higher incorporation efficiency of Al on these facets.

Our previous studies, which include AFM data,[18] show substantial changes to the surface morphology of the as-grown and annealed NLs as the Al content increases. This change in surface morphology led to the suggestion that increasing Al content at the surface might lead to slower diffusion kinetics or a relative reduction in the surface energy of the zb-{111} facets with Al content. This might be responsible for an increasing density of {111} facets, which in turn increase the probability of wz phase formation. Hence, Al segregation to the surface may promote the inclusion of wz regions in the subsequent epilayer even at low average Al contents in the zb film. Since slower decomposition of TMAl is a potential cause of the compositional gradients, slower NL growth rates might be a worthwhile avenue to explore to reduce both these gradients and the formation of wz inclusions.

IV. CONCLUSION

The origins of the wurtzite inclusions observed in GaN epilayers grown over AlGaN NLs were studied using electron microscopy. The GaN NL and the $Al_{0.95}Ga_{0.05}N$ NL were initially highly zincblende and wurtzite in phase, respectively, which is thought to be related to the much larger energy difference between the zincblende and wurtzite structures in AlN as compared to GaN. These phases continued to grow into the overgrown GaN epilayer. The zincblende $Al_{0.29}Ga_{0.71}N$ NL with intermediate Al composition led to the formation of wurtzite inclusions in the grown GaN epilayer. These wurtzite inclusions extend from the AlGaN/GaN interface to the surface of GaN epilayer as tilted columnar structures. The NLs exhibit strong {111} faceting, which are probable nucleation sites for wz inclusions in the overgrown GaN epilayers. No significant difference in surface morphology in as-grown and annealed NLs was observed, suggesting that the formation of strong faceting occurs during growth prior to the annealing process. Furthermore, a depletion of Al at the $Al_{0.29}Ga_{0.71}N$ NL/3C-SiC interface was associated with either a delayed incorporation (with slower decomposition) of Al due to longer decomposition times (for its precursor), or a higher Al incorporation efficiency on {111} facets formed with increasing NL thickness.

SUPPLEMENTARY MATERIAL

See the supplementary material for the STEM-EDX measurements of the annealed $Al_{0.29}Ga_{0.71}N$ NL.

ACKNOWLEDGMENTS

We would like to thank the EPSRC for support through Grant Nos. EP/M010589/1 and EP/R01146X/1. D. J. Wallis would like to acknowledge support through the EPSRC fellowship through No. EP/N01202X/2.

AUTHOR DECLARATIONS

Conflict of Interest

The authors have no conflicts to disclose.

DATA AVAILABILITY

The data that support the findings of this study are openly available in the University of Cambridge repository, Ref. 28.

REFERENCES

[1]S. Guha and N. A. Bojarczuk, Appl. Phys. Lett. **72**, 415 (1998).
[2]E. Monroy, E. Muñoz, F. J. Sánchez, F. Calle, E. Calleja, B. Beaumont, P. Gibart, J. A. Muñoz, and F. Cussó, Semicond. Sci. Technol. **13**, 1042 (1998).
[3]S. Nakamura, Rev. Mod. Phys. **87**, 1139 (2015).
[4]L. Y. Lee, Mater. Sci. Tech. **33**(14), 1570 (2017).
[5]A. F. Wright, J. Appl. Phys. **82**, 2833 (1997).
[6]T. Hanada, "Basic properties of ZnO, GaN, and related materials," in *Oxide and Nitride Semiconductors—Processing, Properties, and Applications*, Advances in Materials Research Vol. 12, edited by T. Yao, and S.-K. Hong (Springer, Berlin, 2009).
[7]P. Vacek, M. Frentrup, L. Y. Lee, F. C.-P. Massabuau, M. J. Kappers, D. J. Wallis, R. Gröger, and R. A. Oliver, J. Appl. Phys. **129**, 155306 (2021).
[8]E. Kimura, T. Suzuki, M. Ouchi, K. Ishida, and K. Takahashi, J. Cryst. Growth **278**, 411 (2005).
[9]J. N. Kuznia, J. W. Yang, Q. C. Chen, S. Krishnankutty, M. A. Khan, T. George, and J. Frietas Jr., Appl. Phys. Lett. **65**(19), 2407994 (1994).
[10]H. Yang, L. X. Zheng, J. B. Li, X. J. Wang, D. P. Xu, Y. T. Wang, X. W. Hu, and P. D. Han, Appl. Phys. Lett. **74**(17), 2498 (1999).
[11]S. Strite, J. Ruan, Z. Li, A. Salvador, H. Chen, D. J. Smith, W. J. Choyke, and H. Morkoç, J. Vac. Sci. Technol. B **9**(4), 1924 (1991).
[12]A. Trampert, O. Brandt, H. Yang, and K. H. Ploog, Appl. Phys. Lett. **70**(5), 583 (1997).
[13]H. Okumura, K. Ohta, G. Feuillet, K. Balakrishnan, S. Chichibu, H. Hamaguchi, P. Hacke, and S. Yoshida, J. Cryst. Growth **178**, 113 (1997).
[14]D. J. As, J. Microelectron. **40**, 204 (2009).
[15]D. Gerthsen, B. Neubauer, C. H. Dieker, R. Lantier, A. Rizzi, and H. Lüth, J. Cryst. Growth **200**, 353 (1999).
[16]L. Y. Lee, M. Frentrup, M. J. Kappers, R. A. Oliver, C. J. Humphreys, and D. J. Wallis, J. Appl. Phys. **124**(10), 105302 (2018).
[17]D. Zu, D. J. Wallis, and C. J. Humphreys, Rep. Pro. Phys. **76**(10), 106501 (2013).
[18]A. Gundimeda, M. Rostami, M. Frentrup, A. Hinz, M. J. Kappers, D. J. Wallis, and R. A. Oliver, J. Phys. D **55**, 175110 (2022).
[19]K. Lorenz, M. Gonsalves, W. Kim, V. Narayanan, and S. Mahajan, Appl. Phys. Lett. **77**, 3391 (2000).
[20]C. H. Wei, Z. Y. Xie, L. Y. Li, Q. M. Yu, and J. H. Edgar, J. Electron. Mater. **29**, 317 (2000).
[21]M. Frentrup, L. Y. Lee, S.-L. Sahonta, M. J. Kappers, F. Massabuau, P. Gupta, R. A. Oliver, C. J. Humphreys, and D. J. Wallis, J. Phys. D **50**(43), 433002 (2017).
[22]D. N. Johnstone, P. Crout, M. Nord, and J. Laulainen (2021). "Pyxem/Pyxem: Pyxem 0.13.2 (Version v0.13.2)," Zenodo. https://doi.org/10.5281/zenodo.4687011
[23]L. Y. Lee, M. Frentrup, P. Vacek, M. J. Kappers, D. J. Wallis, and R. A. Oliver, J. Appl. Phys. **125**(10), 105303 (2019).
[24]M. Städele, J. A. Majewski, and P. Vogl, Phys. Rev. B **56**(11), 6911 (1997).
[25]J. Stellmach, M. Pristovsek, Ö. Savaş, J. Schlegel, E. V. Yakovlev, and M. Kneissl, J. Cryst. Growth **315**(1), 229 (2011).
[26]K. M. Mazaev, A. V. Lobanova, E. V. Yakovlev, R. A. Talalaev, A. O. Galyukov, Y. N. Makarov, D. Gotthold, B. Albert, L. Kadinski, and B. Peres, J. Cryst. Growth **261**(2–3), 190 (2004).
[27]T. G. Mihopoulos, V. Gupta, and K. F. Jensen, J. Crystal Growth **195**, 733 (1998).
[28]A. Gundimeda, M. Frentrup, S. M. Fairclough, M. J. Kappers, D. J. Wallis, and R. A. Oliver (2022). Research data supporting "Investigation of wurtzite formation in MOVPE-grown zincblende GaN epilayers on $Al_xGa_{1-x}N$ nucleation layers," University of Cambridge repository. https://doi.org/10.17863/CAM.81573